Research Article | Vol. 26, No. 3 | 5 Feb 2018 | OPTICS EXPRESS 3674
Optics EXPRESS

Impact of substrate etching on plasmonic elements and metamaterials: preventing red shift and improving refractive index sensitivity

YUTO MORITAKE[1] AND TAKUO TANAKA[1,2,3,*]

[1]*Innovative Photon Manipulation Research Team, RIKEN Center for Advanced Photonics, RIKEN, Japan*
[2]*Metamaterials Laboratory, RIKEN, Japan*
[3]*School of Materials and Chemical Technology, Tokyo Institute of Technology, Japan*
**t-tanaka@riken.jp*

Abstract: We propose and demonstrate the elimination of substrate influence on plasmon resonance by using selective and isotropic etching of substrates. Preventing the red shift of the resonance due to substrates and improving refractive index sensitivity were experimentally demonstrated by using plasmonic nanostructures fabricated on silicon substrates. Applying substrate etching decreases the effective refractive index around the metal nanostructures, resulting in elimination of the red shift. Improvement of sensitivity to the refractive index environment was demonstrated by using plasmonic metamaterials with Fano resonance based on far field interference. Change in quality factors (Q-factors) of the Fano resonance by substrate etching was also investigated in detail. The presence of a closely positioned substrate distorts the electric field distribution and degrades the Q-factors. Substrate etching dramatically increased the refractive index sensitivity reaching to 1532 nm/RIU since the electric fields under the nanostructures became accessible through substrate etching. The FOM was improved compared to the case without the substrate etching. The method presented in this paper is applicable to a variety of plasmonic structures to eliminate the influence of substrates for realizing high performance plasmonic devices.

OCIS codes: (160.3918) Metamaterials; (220.4241) Nanostructure fabrication; (240.6680) Surface plasmons; (260.5740) Resonance; (280.1415) Biological sensing and sensors; (250.5403) Plasmonics; (310.6628) Subwavelength structures, nanostructures.

References and links

1. M. D. Mailnsky, K. L. Kelly, G. C. Schatz, and R. P. Van Duyne, "Nanosphere Lithography: Effect of Substrate on the Localized Surface Plasmon Resonance Spectrum of Silver Nanoparticles," J. Phys. Chem. B **105**(12), 2343–2350 (2001).
2. A. Curry, G. Nusz, A. Chilkoti, and A. Wax, "Substrate effect on refractive index dependence of plasmon resonance for individual silver nanoparticles observed using darkfield microspectroscopy," Opt. Express **13**(7), 2668–2677 (2005).
3. K. C. Vernon, A. M. Funston, C. Novo, D. E. Gómez, P. Mulvaney, and T. J. Davis, "Influence of particle-Substrate Interaction on Localized Plasmon Resonances," Nano Lett. **10**(6), 2080–2086 (2010).
4. E. Ringe, J. M. McMahon, K. Sohn, C. Cobley, Y. Xia, J. Huang, G. C. Schatz, L. D. Marks, and R. P. Van Duyne, "Unraveling the Effects of Size, Composition, and Substrate on the Localized Surface Plasmon Resonance Frequencies of Gold and Silver Nanocubes: A Systematic Single-Particle Approach," J. Phys. Chem. C **114**(29), 12511–12516 (2010).
5. L. Novotny, "Effective Wavelength Scaling for Optical Antennas," Phys. Rev. Lett. **98**(26), 266802 (2007).
6. X. Xu, B. Peng, D. Li, J. Zhang, L. M. Wong, Q. Zhang, S. Wang, and Q. Xiong, "Flexible Visible-Infrared Metamaterials and Their Applications in Highly Sensitive Chemical and Biological Sensing," Nano Lett. **11**(8), 3232–3238 (2011).
7. R. Hokari, Y. Kanamori, and K. Hane, "Comparison of electromagnetically induced transparency between silver, gold, and aluminum metamaterials at visible wavelengths," Opt. Express **22**(3), 3526–3537 (2014).
8. A. Dmitriev, C. Hägglund, S. Chen, H. Fredriksson, T. Pakizeh, M. Käll, and D. S. Sutherland, "Enhanced Nanoplasmonic Optical Sensors with Reduced Substrate Effect," Nano Lett. **8**(11), 3893–3898 (2008).

#315041 https://doi.org/10.1364/OE.26.003674
Journal © 2018 Received 6 Dec 2017; revised 25 Jan 2018; accepted 26 Jan 2018; published 2 Feb 2018

Optics EXPRESS

9. M. A. Otte, M.-C. Estévez, L. G. Carrascosa, A. B. González-Guerrero, L. M. Lechuga, and B. Sepúlveda, "Improved Biosensing Capability with Novel Suspended Nanodisks," J. Phys. Chem. C **115**(13), 5344–5351 (2011).
10. S. S. Aćimović, H. Šípová, G. Emilsson, A. B. Dahlin, T. J. Antosiewicz, and M. Käll, "Superior LSPR substrates based on electromagnetic decoupling for on-a-chip high-throughput label-free biosensing," Light Sci. Appl. **6**(8), e17042 (2017).
11. C.-C. Chen, A. Ishikawa, Y.-H. Tang, M.-H. Shiao, D. P. Tsai, and T. Tanaka, "Uniaxial-isotropic Metamaterials by Three-Dimensional Split-Ring Resonators," Adv. Opt. Mater. **3**(1), 44–48 (2015).
12. Y. Moritake and T. Tanaka, "Controlling bi-anisotropy in infrared metamaterials using three-dimensional split-ring-resonators for purely magnetic resonance," Sci. Rep. **7**(1), 6726 (2017).
13. R. B. Johnson and R. W. Christy, "Optical Constants of the Nobel Metals," Phys. Rev. B **6**(12), 4370–4379 (1972).
14. J. N. Anker, W. P. Hall, O. Lyandres, N. C. Shah, J. Zhao, and R. P. Van Duyne, "Biosensing with plasmonic nanosensors," Nat. Mater. **7**(6), 442–453 (2008).
15. K. M. Mayer and J. H. Hafner, "Localized Surface Plasmon Resonance Sensors," Chem. Rev. **111**(6), 3828–3857 (2011).
16. B. Luk'yanchuk, N. I. Zheludev, S. A. Maier, N. J. Halas, P. Nordlander, H. Giessen, and C. T. Chong, "The Fano resonance in plasmonic nanostructures and metamaterials," Nat. Matter. 707 (2010).
17. J. A. Fan, K. Bao, C. Wu, J. Bao, R. Bardhan, N. J. Halas, V. N. Manoharan, G. Shvets, P. Nordlander, and F. Capasso, "Fano-like interference in Self-Assembled Plasmonic Quadrumer Clusters," Nano Lett. **10**(11), 4680–4685 (2010).
18. N. Liu, T. Weiss, M. Mesch, L. Langguth, U. Eigenthaler, M. Hirscher, C. Sönnichsen, and H. Giessen, "Planar Metamaterial Analogue of Electromagnetically Induced Transparency for Plasmonic Sensing," Nano Lett. **10**(4), 1103–1107 (2010).
19. N. Verellen, P. Van Dorpe, C. Huang, K. Lodewijks, G. A. E. Vandenbosch, L. Lagae, and V. V. Moshchalkov, "Plasmon Line Shaping Using Nanocrosses for High Sensitivity Localized Surface Plasmon Resonance Sensing," Nano Lett. **11**(2), 391–397 (2011).
20. C. Wu, A. B. Khanikaev, R. Adato, N. Arju, A. A. Yanik, H. Altug, and G. Shvets, "Fano-resonant asymmetric metamaterials for ultrasensitive spectroscopy and identification of molecular monolayers," Nat. Mater. **11**(1), 69–75 (2011).
21. F. Cheng, X. Yang, and J. Gao, "Ultrasensitive detection and characterization of molecules with infrared plasmonic metamaterials," Sci. Rep. **5**(1), 14327 (2015).
22. N. Liu, L. Langguth, T. Weiss, J. Kästel, M. Fleischhauer, T. Pfau, and H. Giessen, "Plasmonic analogue of electromagnetically induced transparency at the Drude damping limit," Nat. Mater. **8**(9), 758–762 (2009).
23. V. A. Fedotov, M. Rose, S. L. Prosvirnin, N. Papasimakis, and N. I. Zheludev, "Sharp Trapped-Mode Resonances in Planar Metamaterials with a Broken Structural Symmetry," Phys. Rev. Lett. **99**(14), 147401 (2007).
24. B. Lahiri, A. Z. Khokhar, R. M. De La Rue, S. G. McMeekin, and N. P. Johnson, "Asymmetric split ring resonators for optical sensing of organic materials," Opt. Express **17**(2), 1107–1115 (2009).
25. N. E. J. Omaghali, V. Tkachenko, A. Andreone, and G. Abbate, "Optical Sensing Using Dark Mode Excitation in an Asymmetric Dimer Metamaterial," Sensors (Basel) **14**(1), 272–282 (2013).
26. Y. Moritake, Y. Kanamori, and K. Hane, "Experimental demonstration of sharp Fano resonance in optical metamaterials composed of asymmetric double bars," Opt. Lett. **39**(13), 4057–4060 (2014).
27. Y. Moritake, Y. Kanamori, and K. Hane, "Emission wavelength tuning of fluorescence by fine structural control of optical metamaterials with Fano resonance," Sci. Rep. **6**(1), 33208 (2016).
28. N. Papasimakis and N. I. Zheludev, "Metamaterial induced transparency: Sharp Fano resonances and slow light," Opt. Photonics News **20**(10), 22–27 (2009).
29. R. Singh, C. Rockstuhl, F. Lederer, and W. Zhang, "The impact of nearest neighbor interaction on the resonances in terahertz metamaterials," Appl. Phys. Lett. **94**(2), 021116 (2009).
30. C. Ropers, D. J. Park, G. Stibenz, G. Steinmeyer, J. Kim, D. S. Kim, and C. Lienau, "Femtosecond Light Transmission and Subradiant Damping in Plasmonic Crystals," Phys. Rev. Lett. **94**(11), 113901 (2005).
31. A. Christ, Y. Ekinci, H. H. Solak, N. A. Gippius, S. G. Tikhodeev, and O. J. F. Martin, "Controlling the Fano interference in a plasmonic lattice," Phys. Rev. B **76**(20), 201405 (2007).
32. F. Hao, P. Nordlander, Y. Sonnefraud, P. Van Dorpe, and S. A. Maier, "Tunability of Subradiant Dipolar and Fano-Type Plasmon Resonances in Metallic Ring/Disk Cavities: Implications for Nanoscale Optical Sensing," ACS Nano **3**(3), 643–652 (2009).
33. L. J. Sherry, R. Jin, C. A. Mirkin, G. C. Schatz, and R. P. Van Duyne, "Localized Surface Plasmon Resonance Spectroscopy of Single Silver Triangular Nanoprisms," Nano Lett. **6**(9), 2060–2065 (2006).
34. A. J. Haes and R. P. Van Duyne, "A nanoscale Optical Biosensor: Sensitivity and Selectivity of an Approach Based on the Localized Surface Plasmon Resonance Spectroscopy of Triangular Silver Nanoparticles," J. Am. Chem. Soc. **124**(35), 10596–10604 (2002).
35. P. Offermans, M. C. Schaafsma, S. R. Rodriguez, Y. Zhang, M. Crego-Calama, S. H. Brongersma, and J. Gómez Rivas, "Universal Scaling of the Figure of Merit of Plasmonic Sensors," ACS Nano **5**(6), 5151–5157 (2011).

Optics EXPRESS

36. A. Danilov, G. Tselikov, F. Wu, V. G. Kravets, I. Ozerov, F. Bedu, A. N. Grigorenko, and A. V. Kabashin, "Ultra-narrow surface lattice resonances in plasmonic metamaterial arrays for biosensing applications," Biosens. Bioelectron. **104**, 102–112 (2017).

1. Introduction

Understanding the influence of substrates on plasmons is crucial since metal nanostructures exhibiting plasmon resonance are generally fabricated on a substrate. The optical properties of plasmon modes are sensitive to the surrounding environment so that their properties are easily modified by the presence of a substrate, which is often unwanted for applications using plasmons. For example, the presence of a substrate induces a red shift of the resonant wavelengths [1–4]. Therefore, based on a scaling rule in electromagnetics [5–7], miniaturization of the structures is necessary for the resonant wavelengths to be the designed values after the red shift and this miniaturization makes fabrication more difficult. Another example is restriction of the available electromagnetic fields around the metal nanostructures. Significant portions of the near fields around the metal nanostructures are inaccessible due to the substrate, but these near fields are essential for plasmonic devices. So far, several methods to reduce substrate influence for improvement of sensitivity have been published by using dipolar plasmon resonance [8–10].

In this paper, we propose and demonstrate the elimination of substrate influence on plasmonic elements by using selective and isotropic etching of substrates. The concept of the substrate etching is shown in Fig. 1. After forming the metal nanostructures on the substrate, only the substrate is etched via selective etching. Employing an isotropic etching condition, the substrate underneath the structures is removed, resulting in reduction of the surrounding refractive index and extension of the available near fields as shown in Fig. 1. As a result, the red shift due to the substrate is eliminated and refractive index sensitivity is improved.

This paper is divided into two parts: prevention of the red shift and improvement of refractive index sensitivity. First, we demonstrate the concept of substrate etching by using gold bars formed on a silicon substrate. Elimination of the substrate-induced red shift is investigated experimentally and numerically. The plasmon resonant wavelengths approach the intrinsic wavelength without any influence from the substrate due to the dipolar nature of the plasmon modes. In the next step, plasmonic metamaterials with Fano resonance is used to demonstrate improvement of refractive index sensitivity. In addition to the resonant wavelengths, the impact of substrate etching on quality factors (Q-factors), which is an important parameter for sensitivity, is also investigated. By applying the substrate etching, high refractive index sensitivity reaching to 1537 nm/RIU and improvement of FOM is achieved.

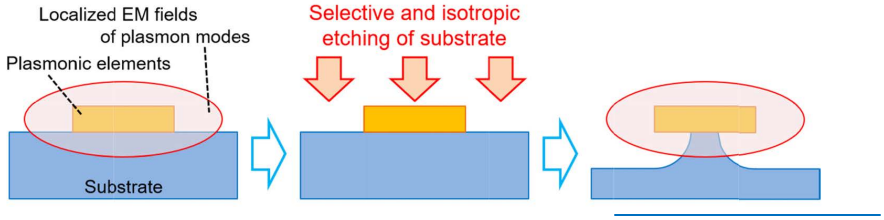

Fig. 1. Schematic of substrate etching for plasmonic elements formed on a substrate. By selective and isotropic etching, the substrate underneath the metal nanostructure is removed and influence of the substrate on the plasmonic modes is eliminated.

2. Preventing red shift due to substrate

To demonstrate prevention of red shift due to the substrate, we applied substrate etching to gold bar structures fabricated on a silicon substrate as shown in Fig. 2. While a silicon substrate is frequently used in the near infrared region owing to its transparency, the high index of silicon, which is around 3.4, affects resonant properties of plasmonic elements such

Optics EXPRESS

as unwanted red shift of resonant wavelength. The bar length L, width W, and periodicity along both directions $P = P_x = P_y$ are 600, 200, and 1000 nm, respectively. The gold bars were fabricated by a conventional lift-off method using electron beam lithography and electron beam evaporation of 60 nm-thick-gold. Before deposition of gold, buffered hydro fluid treatment was performed to get better adhesion between silicon and gold. After forming the structures on the silicon substrate, inductive coupled plasma reactive ion etching (ICP-RIE, SAMCO, RIE200iPT) was performed with parameters of CF_4 plasma of flow rate of 20 sccm, pressure of 0.15 Pa, ICP power of 500 W, and forward power of 0 W. By setting forward power to 0 W, only the silicon substrate was isotropically etched [11,12]. Figures 3(a)-3(e) show the scanning electron microscope (SEM) images of the fabricated gold bars with increasing etching time. The etched thickness T_{etch} measured by a surface profiler linearly increases with T_{etch} as shown in Fig. 3(f). Here, T_{etch} is defined as the depth of etched silicon surface from the initial surface as shown in Fig. 4(c). It is observed from the SEM images that the silicon substrate underneath the gold bars is isotropically etched.

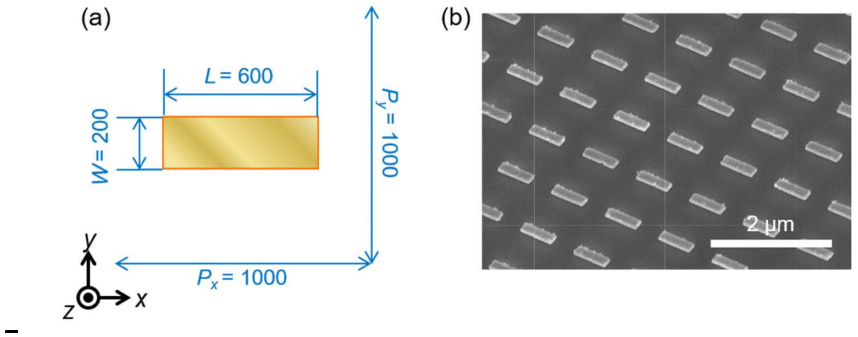

Fig. 2. (a) Schematic of the gold bar (Unit: nm) and (b) the SEM image of the fabricated gold bars on the silicon substrate.

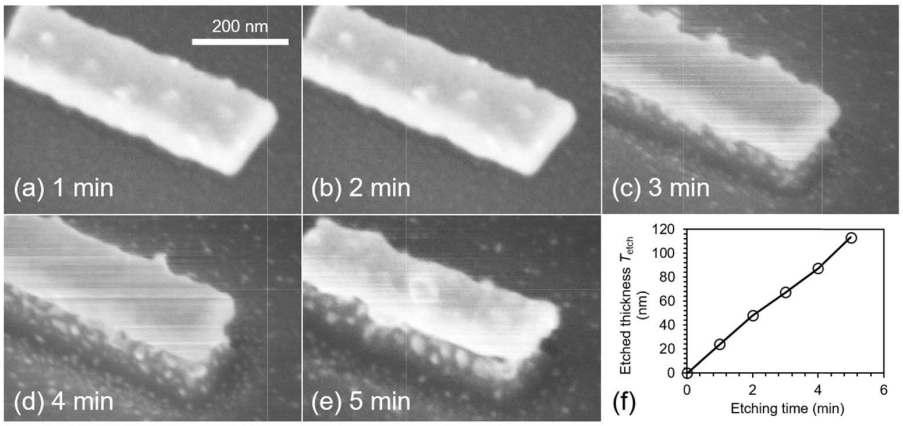

Fig. 3. (a)-(e) The SEM images of the gold bars at the respective etching time. (f) Relationship between etching time and etched thickness T_{etch}.

Transmission spectra measured by the Fourier transform infrared (FT-IR) spectrometer (JASCO system FT/IR-6300FV) are shown in Fig. 4(a). Incidence was normal to a substrate and its polarization direction was along to the bars. All experimental spectra presented in this paper are normalized by the bare silicon substrate with around 70% transmission so that some values of transmission exceed 100%. The dips due to the plasmon resonance are clearly seen in all spectra. The experimental resonant wavelength shift as a function of T_{etch} is shown as black hollow circles in Fig. 4(b). The resonant wavelengths shift from 3.65 μm to 1.71 μm as

Optics EXPRESS

the etching time increases and finally saturates at the etching time of 4 min. This blue shift originates from the reduction of the effective refractive index around the gold bars. Through substrate etching, the resonant wavelengths become less than half (1.71 / 3.65 ~0.47) without miniaturization of the structures. Additionally, the resonant wavelength shift shows linear dependence on T_{etch} until saturation, which is useful for resonant wavelength tuning after fabrication of structures on a substrate.

To investigate substrate etching numerically, simulations based on the finite element method (FEM) were carried out using commercial software (COMSOL). The calculation model is shown in Fig. 4(c). In the simulations, isotropic etching of the silicon substrates was assumed. Since naturally oxidized layer on the etched silicon surface was confirmed by ellipsometry before FTIR measurements, a 3 nm-thick natural oxide layer on the silicon surfaces were considered. The dielectric function of gold in Ref [13]. was used. The refractive index of silicon and silicon dioxide were set to 3.4 and 1.45, respectively, which are typical values in this wavelength region. The simulated resonant wavelength shift as a function of T_{etch} is shown by the blue hollow squares in Fig. 4(b) and agrees well with experiments. The resonant wavelength of the gold bars floating in air was also simulated to find the saturation point, which is indicated by the red solid line in Fig. 4(b). Surprisingly, the resonant wavelengths of the gold bars after applying substrate etching converge to that of the gold bars floating in air, indicating that substrate etching eliminates the influence of the substrate on the resonant wavelengths. From the normalized electric field distributions in the case of T_{etch} = 0 and 95 nm shown in Fig. 4(d), the electric fields are concentrated at the edges of the bars since the excited plasmon modes have a dipolar nature. This may be the reason why the gold bars feel negligible influence from the remaining silicon pillars. Under the assumption of isotropic etching used in the simulations, the silicon pillar underneath the metal structures is completely removed when the etched thickness T_{etch} exceeds 100 nm. However, in the experiments, the gold bars are still anchored to the substrate although T_{etch} reached to 113.5 nm. This means that the etching rate along the lateral direction would be a little lower than that along the depth direction.

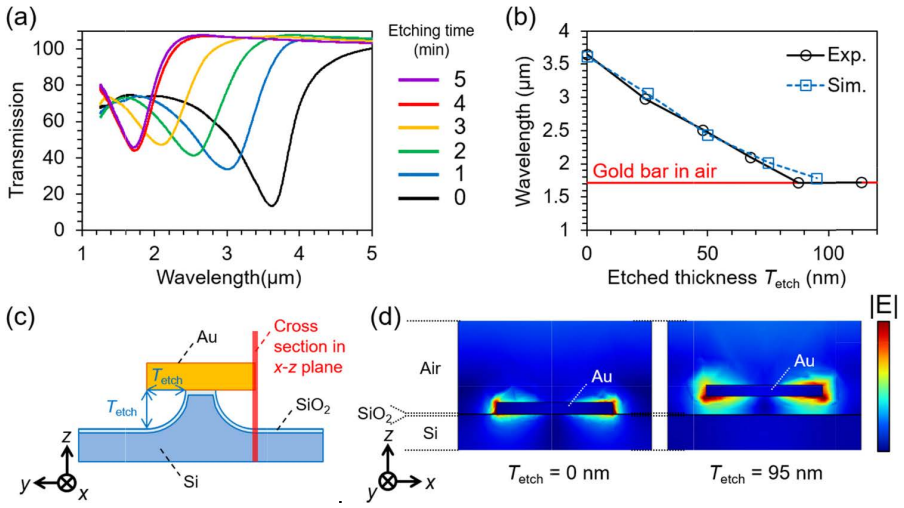

Fig. 4. (a) The transmission spectra for the gold bars while varying the etching time. (b) The plasmon resonant wavelengths as a function of the etched thickness T_{etch}. The black hollow circles and blue hollow squares correspond to experiments and simulations, respectively. The red line indicates the resonant wavelength of gold bars floating in air. (c) The model used in simulations. (d) The normalized electric field distributions at the plasmon resonance in the case of T_{etch} = 0 and 95 nm. The cross section is indicated in (c).

Optics EXPRESS

3. Improving refractive index sensitivity

To demonstrate improvement of refractive index sensitivity, we used plasmonic metamaterials with Fano resonance and investigated their refractive index sensitivity after applying substrate etching. Chemical and biological sensors are one of the promising applications in plasmonics [14,15]. Utilizing the plasmon modes' high sensitivity to the surrounding index environment enables us to detect a tiny amount of analyte by their resonant wavelength shift. Releasing the near fields under the nanostructures through substrate etching gives rise to improvement of the plasmon modes' sensitivity to the surrounding refractive index. So far, similar methods have been reported to enhance sensitivity of dipolar localized plasmons in metal elements for bio-sensing [8–10]. The main difference from these preceding works is that Fano resonance in plasmonic metamaterials is utilized instead of dipolar localized plasmon resonance. Fano resonance results from the interference between optically bright and dark modes. Since the dark modes have high Q-factors due to small radiation loss, refractive index sensitivity of Fano resonance is higher than that of dipolar localized plasmon resonance [16–21].

Plasmonic nanostructures exhibiting Fano resonance can be categorized into two types. One is based on the near field coupling between bright and dark modes [22], and the other is based on the destructive interference of the far fields radiated by dark modes with broken symmetry [23]. In the case of Fano resonance based on near field coupling, realization of the Fano resonance strongly depends on the coupling condition between bright and dark plasmon modes. Since the coupling condition is sensitive to the refractive index environment around the nanostructures, high sensitivity can be achieved. However, very large refractive index change breaks the coupling condition and the Fano resonance disappears. On the other hand, Fano resonance based on far field interference is adaptive to the substrate etching since it does not depend on near field coupling [24]. Therefore, in this study, we chose the Fano resonance based on the far field interference using asymmetric double bar (ADB) metamaterials [25–27]. The ADB is composed of two gold bars with slightly different bar lengths as shown in Fig. 5. Knowledge of substrate etching for the gold bars discussed in the previous section is applicable to ADB since the ADB is also composed of gold bars. The Fano resonance in ADB metamaterials occurs by the interference between the in-phase mode and the anti-phase mode that are formed via hybridization of the coupled two dipolar plasmon modes at the gold bars. In the in- (anti-) phase mode, two dipolar plasmons at the bars oscillate in phase (anti-phase). The in-phase mode has a large total dipole moment and large radiation loss. On the other hand, the anti-phase mode has small radiation loss since the anti-phase oscillation of the two dipolar plasmon modes gives rise to the destructive interference in the far fields [28]. Therefore, the in-phase (anti-phase) mode works as a bright (dark) mode. The length difference allows excitation of the anti-phase mode, resulting in sharp Fano resonance. Since the Fano resonance in ADB metamaterials is based on the interference between the far field radiations, substrate etching does not destroy the Fano resonance. Diffractive coupling among unit cells is also important for characteristics of Fano resonance. Singh *et al.* showed diffractive coupling can enhance the Q-factors by changing the period of unit cells [29]. However, the period of the ADB metamaterials in this work is small enough that the diffractive coupling doesn't play important role for characteristics of Fano resonance.

Experimental investigation using the ADB metamaterials was done by the same procedure as the gold bars. The design of the ADB structures is shown in Fig. 5(a). The lengths of the long and short bar L_1, L_2 are 600 and 480 nm, respectively. The width W and gap G of the bars are both 200 nm. The periodicity along both directions $P = P_x = P_y$ is 1000 nm. The ADB metamaterial was fabricated by a lift-off method and the substrate etching procedure was same as the gold bars mentioned in the previous section. The SEM image of the fabricated ADB metamaterial is shown in Fig. 5(b). From FTIR measurements for the ADB metamaterial formed on the silicon substrate, the broad dips due to the in-phase mode and the asymmetric spectral responses due to the Fano resonance are observed at around 3.0 μm and

Optics EXPRESS

3.7 μm [black line in Fig. 6(a)], respectively. Use of the substrate etching causes a blue shift of the resonant wavelength – a trend similarly observed with the gold bars.

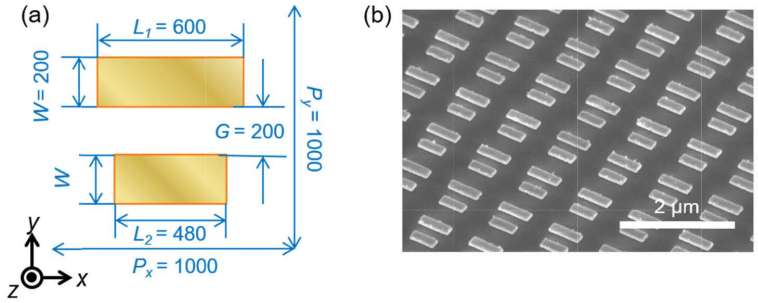

Fig. 5. (a) Schematic of the ADB structure (Unit: nm) and (b) the SEM image of the fabricated ADB metamaterial on the silicon substrate.

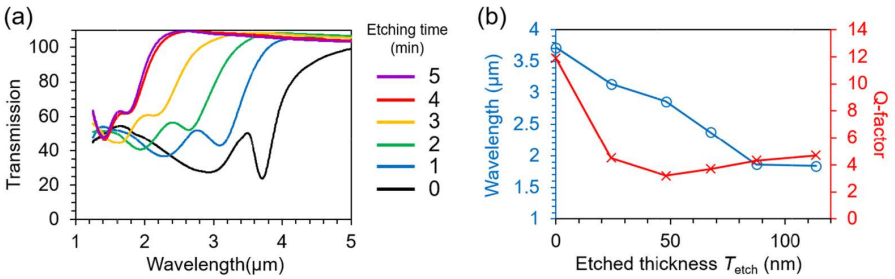

Fig. 6. (a) The transmission spectra for the ADB metamaterial while varying the etching time. (b) The Fano resonant wavelengths (blue hollow circles, left axis) and the Q-factors (red crosses, right axis) as a function of etched thickness T_{etch}.

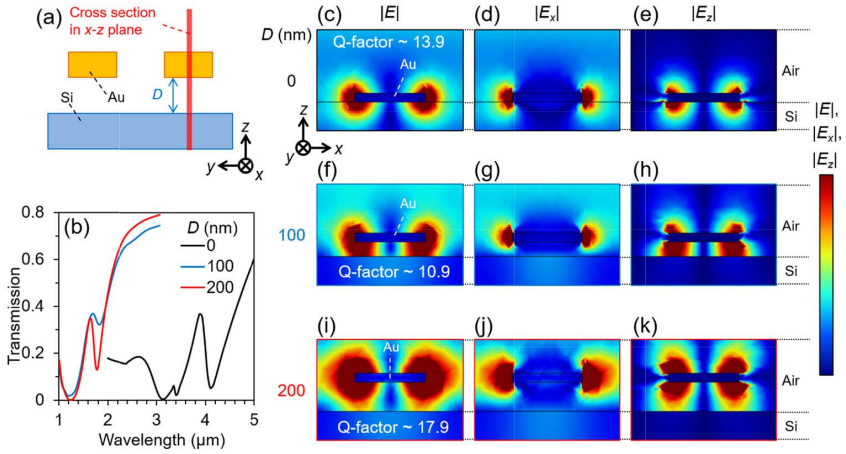

Fig. 7. (a) The simulated model for investigating substrate influence on Q-factors. (b) The simulated transmission spectra changing the distance between the ADB structures and the substrate D. The normalized electric field distributions at the Fano resonance in the case of D = (c)-(e) 0, (f)-(h) 100, (i)-(k) 200 nm. (c), (f), (i) are the absolute value of electric fields. (d), (g), (j) are the x-component of the electric fields. (e), (h), (k) are the z-component of electric fields. The cross-sectional plane is indicated in (a).

To investigate influence of substrate etching on the characteristics of the Fano resonance, the resonant wavelengths and quality factors (Q-factors) are extracted by fitting using a

Optics EXPRESS

phenomenological formula for Fano resonance [30–32]. The Q-factor is λ / FWHM, where λ is the resonant wavelength. Figure 6(b) shows the resonant wavelengths and Q-factors as a function of the etched thickness T_{etch} by the blue hollow circles and red crosses, respectively. The resonant wavelengths of the Fano resonance shift from 3.72 μm to 1.84 μm, and the ratio 1.84 / 3.72 equals to ~0.49 which is almost same as the case of the gold bars. The Q-factors shows an interesting behavior with change in T_{etch}; the Q-factors first drop from 11.9 to 4.51, and then slightly increase with T_{etch}.

For a better understanding of the observed change in the Q-factors, effects of the substrate apart from the ADB structures with the distance D were numerically investigated using the simplified model shown in Fig. 7(a). Except for absence of the silicon pillar under the gold structures, the situation in the model is nearly the same as the realistic structures after applying substrate etching. Figure 7(b) shows simulated transmission spectra for D = 0, 100, 200 nm. In the case of D = 100, 200 nm, since the substrate has negligible influence on the resonant wavelengths, the Fano resonant wavelengths shift to the intrinsic resonant wavelength for the ADB metamaterial surrounded by air. The extracted Q-factors are 13.9, 10.9, and 17.9 for D = 0, 100, and 200 nm, respectively. Interestingly, the Q-factors of the Fano resonance for D = 100 nm is smaller than those for D = 0 and 200 nm. To explain the reduction of the Q-factors at D = 100 nm, the normalized electric field distributions at the Fano resonance are plotted as shown in Figs. 7(c)-7(k). In the case of D = 100 nm, the presence of the substrate makes the electric field distribution more asymmetrical with respect to the bars, while the electric fields are symmetrical for D = 0 and 200 nm. The asymmetry of the fields originates from the distortion of the z-components of the electric fields as shown in Fig. 7(h), which means polarization charges are induced at the substrate surface and attract the electric fields [3]. The distortion of the electric fields by the substrate would degrade the Fano resonance and reduce the Q-factors. Since the refractive index of silicon is relatively high, the induced polarization becomes large enough to degrade the Fano resonance. This degradation was not observed in the case of a silicon dioxide substrate with refractive index of 1.45, which was confirmed by simulations (not shown). Since D is less than 100 nm in the experiments, the Q-factors decrease after applying substrate etching and gradually improve with increase of the distance from the substrate. For eliminating the influence of the substrate on the Q-factors, use of lower index substrates or setting an optimal distance between the structures and the substrate is necessary.

To investigate refractive index sensitivity of the Fano resonance in the ADB metamaterial with substrate etching, polymethyl methacrylate (PMMA) was spin-coated on the ADB metamaterial. The thickness of the PMMA layer was ~200 nm. Figure 8(a) shows the measured transmission spectra for the ADB metamaterial with the substrate etching before/after the PMMA coating. The PMMA coating induces a red shift of the Fano resonance's resonant wavelength from 1.84 μm to 2.59 μm and their ratio 2.59 / 1.84 equals to ~1.41. This value is close to 1.49: typical value of refractive index of PMMA in this wavelength region [24], which indicates that the influence of the substrate on the Fano resonant wavelengths was almost eliminated before the PMMA coating.

To show an advantage of substrate etching over miniaturized structures with the same resonant wavelength, the ADB metamaterial with a smaller size was also fabricated [inset of Fig. 8(b)] and its refractive index sensitivity was investigated. All structural parameters of the miniaturized sample are 0.425 times smaller so that the resonant wavelength of the Fano resonance becomes close to that of the ADB metamaterial with the substrate etching. Hereafter, we call the ADB metamaterial sample after applying the substrate etching and the miniaturized sample as ADB-etch and ADB-non, respectively. Figure 8(b) shows the results of sensitivity experiments for the ADB-non. The Fano resonance at 1.61 μm is shifted to 1.70 μm after PMMA coating and the ratio 1.70 / 1.61 is ~1.06, which means effective refractive index around the structures does not significantly change due to the presence of the substrate.

Optics EXPRESS

To evaluate the sensing performance of plasmon sensors, several measures are generally used. Here, we calculate the Q-factors, sensitivity, and FOM from transmission spectra. The sensitivity is defined as the wavelength shift divided by change in effective refractive index around gold structures (nm/RIU). The values of effective refractive index change by PMMA coating are 0.49 and 0.25 for ADB-etch and ADB-non, respectively. The effective refractive index for ADB-non is calculated by averaging the indices of silicon substrate and cover layer. The FOM is calculated by dividing the sensitivity by a FWHM of the resonance (1/RIU) [33]. These parameters extracted from the experimental spectra are summarized in Table 1. Before the PMMA coating, ADB-non had a higher Q-factor than that of ADB-etch since the substrate etching reduces the Q-factors of the Fano resonance as shown in Fig. 6(b). Improvement of the Q-factors by PMMA coating can be qualitatively understood by the electric field distortion discussed previously. A PMMA layer mitigates the high index contrast between air and silicon substrate since the index of PMMA (1.49) is in between that of air (1) and silicon (3.4), making the electric field distributions more symmetric. In terms of the sensitivity, ADB-etch shows dramatic improvement reaching to 1537 nm/RIU compared with ADB-non. The improvement of the sensitivity exceeding 4 times by using substrate etching is attributed to the extension of accessible electric fields and low index environment around the structures before PMMA coating. Figure 8(c) shows the simulated wavelength shift as a function of the refractive index of the cover layers for ADB-etch and ADB-non. In the simulations for ADB-etch, T_{etch} was set to 95 nm. The sensitivity of ADB-etch and ADB-non calculated from the simulations are 1913 and 822 nm/RIU, respectively. The simulations successfully reproduce the improvement of refractive index sensitivity by substrate etching. The FOM obtained from the experiments are 3.93 and 2.27 for ADB-etch and ADB-non, respectively. Because of the dramatic improvement of the sensitivity, the substrate etching improved the FOM by about 1.7 times despite low Q-factors. These obtained FOM is smaller than preceding studies [17–19, 34–36] mainly due to degradation of Q-factors due to substrate etching. If reduction of the Q-factors by substrate etching is prevented as discussed before, higher FOM is expected. Moreover, there is room for optimization of the performance. For example, changing structural parameters is one possibility since the Q-factors of ADB structures strongly depends on the degree of asymmetry of the structures [26].

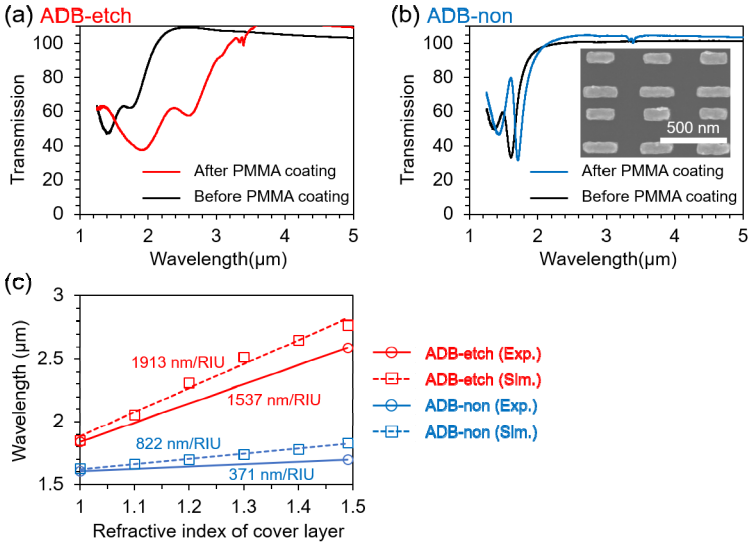

Fig. 8. The transmission spectra before and after PMMA coating for (a) ADB-etch and (b) ADB-non. Inset of (b) is the SEM image of ADB-non. The structural size of ADB-non is smaller than that of ADB-etch by 0.425 times. (c) The wavelength shift as a function of refractive index of the coating layer for ADB-etch (red) and ADB-non (blue). Experiments and simulations are indicated by the circles and squares, respectively.

Optics EXPRESS

Table 1. Refractive index sensing performance of the Fano resonance for ADB-etch and ADB-non.

Sample	Q-factor		Sensitivity (nm/RIU)	FOM
	Bare	With PMMA		
ADB-etch (with substrate etching)	4.70	6.15	1537	3.93
ADB-non (without substrate etching)	9.86	14.6	371	2.27

4. Summary

We proposed and demonstrated elimination of substrate influence on plasmon resonance by using selective and isotropic etching of the substrate. Substrate etching was applied to gold nanostructures on a silicon substrate to show prevention of the red shift and improvement of refractive index sensitivity. The prevention of the red shift was achieved by reduction of effective refractive index around the nanostructures. Surprisingly, substrate influence on the plasmon resonant wavelengths was eliminated since electromagnetic fields are concentrated at the edges of the bars in plasmon resonance. The improvement of refractive index sensitivity was demonstrated by using ADB metamaterials exhibiting Fano resonance based on far field interference. The decrease in the Q-factors of the Fano resonance was observed after applying substrate etching, which was due to the electric field distortion by a closely placed substrate. Optimization of the distance between the nanostructures and the substrate would reduce degradation of the Fano resonance. The sensitivity on refractive index environment of the Fano resonance was enhanced and reached 1532 nm/RIU since the electric fields underneath the nanostructures became accessible through substrate etching. The FOM was also improved by a factor of ~1.7 compared to the miniaturized sample without substrate etching. The method presented in this paper is applicable to a variety of plasmonic structures to eliminate the influence of the substrate for realizing high performance plasmonic devices.

Funding

KAKENHI (17K14128); Japan prize foundation; Innovative Science and Technology Initiative for Security, ATLA, Japan.

Acknowledgments

We would like to thank Dr. M. V. Balois for her English correction.